Bull. Mater. Sci., Vol. 32, No. 2, April 2009, pp. 141–147. © Indian Academy of Sciences.

Low temperature synthesis of nanosized $Mn_{1-x}Zn_xFe_2O_4$ ferrites and their characterizations

RAJESH IYER*, RUCHA DESAI[†] and R V UPADHYAY[††]

Department of Physics, St. Xavier's College, Ahmedabad 380 009, India
[†]Department of Physics, Bhavnagar University, Bhavnagar 364 002, India
[††]Charotar Institute of Applied Sciences, Changa 388 421, India

MS received 28 March 2008

Abstract. **Nanosized $Mn_{1-x}Zn_xFe_2O_4$ (x = 0, 0·1, 0·3, 0·5, 0·6, 0·7, 0·9) mixed ferrite samples of particle size < 12 nm were prepared using the co-precipitation technique by doping the Zn^{2+} ion impurities. Autoclave was employed to maintain constant temperature of 80°C and a constant pressure. The X-ray analysis and the IR spectrum analysis were carried out to confirm the spinel phase formation as well as to ascertain the cation distribution in the ferrite samples. This clearly points to the fact that the Zn^{2+} ion's presence is not restricted to A-site alone for some of the Mn–Zn ferrite series. The real part of a.c. susceptibility measurements clearly indicated the superparamagnetic behaviour of the ferrite samples. There is a systematic decrease in the particle size, Curie temperature and magnetization with the increase in the Zn^{2+} ion doping, measured using magneto thermal gravimetric analysis (MTGA) and vibrating sample magnetometer (VSM), respectively. The lattice constant is found to be constantly decreasing till x = 0·6 and beyond this an unusual slight increase in the lattice constant is found.**

Keywords. **Nanosized mixed ferrites; superparamagnetism; spinel phase.**

1. Introduction

There has been renewed interest in fine magnetic particles with the possibilities of applications in the field of nanostructured materials technology opening up in the last few years (Mostafa *et al* 2006). Due to the large specific area, surface effects might be involved in the magnetism of small particles. Spinel ferrites are extremely important for academic and technological applications. The physical properties of the spinel ferrites such as the electrical, magnetic and elastic properties are governed by the type of magnetic ions residing on the tetrahedral (A) site and octahedral (B) site of the spinel lattice and the relative strength of the inter- and intra-sublattice interactions. This so called cation distribution depends on the chemical composition, the method of preparation, and the cation distribution. In recent years, the design and synthesis of nano-magnetic particles have been the focus of fundamental and applied research owing to their enhanced or unusual properties (Herzer *et al* 2005). It is possible to manipulate the properties of a spinel material to meet the demands of a specific application. Manganese zinc ferrites are technologically important materials because of their high magnetic permeability and low core losses. Ferrites are commonly prepared by a ceramic process involving high temperature solid-state reactions between the constituent oxides/carbonates. The particles obtained by this process are rather large and non-uniform in size. These non-uniform particles, on compacting, result in the formation of voids or low-density area. On sintering, non-reproducible products in terms of their magnetic properties are obtained. In order to overcome difficulties arising out of the ceramic route, wet chemical methods like co-precipitation (Pankov *et al* 1993; Ataie *et al* 1995) have been considered for production of homogeneous, fine and reproducible ferrites.

This paper reports the dependence on cationic stoichiometry of microstructure and magnetic properties of $Mn_{1-x}Zn_xFe_2O_4$ ferrite series (x = 0, 0·1, 0·3, 0·5, 0·6, 0·7, 0·9) prepared at pH 11·5 and a synthesis temperature of 100°C in an autoclave. This temperature of synthesis is lower than the one reported so far (= 180°C) (Jayadevan *et al* 2000; Chandana Rath 2002; Arulmurugan *et al* 2005 have employed co-precipitation method at around 180°C).

The present work is a systematic study of the structural, IR spectroscopy, magnetic of the $Mn_{1-x}Zn_xFe_2O_4$ mixed ferrites, with x = 0, 0·1, 0·3, 0·5, 0·6 and 0·9 having particle size < 12 nm. One of the features of the study is that a non-linear variation of lattice constant has been found. The lattice constant decreases up to x = 0·6 and after that slightly increases for x = 0·7 and 0·9. This is contrary to what has been reported by previous workers. This clearly points to the fact that the Zn^{2+} ion's presence is not restricted to A-site alone for some of the Mn–Zn series. The IR results also further confirm this fact. Here the

*Author for correspondence (rajesh_iyer29@yahoo.com)

magnetization decreases with the decrease in particle size. This is attributed to the fact that Zn^{2+} ions occupy both tetrahedral and octahedral sites in co-precipitated Mn–Zn ferrites (Jayadevan *et al* 2000).

2. Experimental

The co-precipitation technique has been used to produce fine particles of the $Mn_{1-x}Zn_xFe_2O_4$. Initial chemicals used were AR grade $Fe_3Cl_36H_2O$, $MnCl_24H_2O$ and $ZnSO_47H_2O$ salts to obtain the Fe^{3+}, Mn^{2+}, Zn^{2+} and Fe^{2+} ions in an aqueous solution (Upadhyay *et al* 1993). These salts were mixed in required molar ratio in distilled water and added to 8M NaOH solution, under stirring at room temperature for 10 min at 11·5 pH. This precipitated particles were transferred to pre-heated (~ 50°C) autoclave (NOVA Autoclave sterilizer, model no. 8533) and autoclave temperature was raised to a 105 ± 5°C and maintained for 30 min. The aqueous base ferrite nanoparticles were removed from the autoclave and allowed to cool down to room temperature by stirring. Warm water washes were given and finally the precipitation was washed several times with acetone. Wet slurry was kept in an oven for 3 h at 100°C temperature. The dried particles were collected for further characterizations.

2.1 *X-ray diffraction*

X-ray powder diffraction pattern was recorded on a Bruker D-8, X-ray advance Power diffractometer using CuKα radiation (λ = 1·5454 Å). The step size employed was 0·02°, ranging from 25–45°. The average particle size was calculated using Scherrer's formula, using the full width at half maximum intensity for (311) plane of the pattern.

2.2 *Infrared spectroscopy*

The infrared patterns were recorded using infrared spectrometer Thermonicolet IR200 in the range 40,000–120,000 m^{-1}. The samples were prepared in the form of pellets in the KBr medium. The ratio of KBr to the specimen was kept at 1 : 100.

Table 1. Lattice constant and particle size of the $Mn_{1-x}Zn_xFe_2O_4$ ferrites.

Sample	A-site	B-site
Mz0	$(Mn^{+2}_{0.7}Fe^{+3}_{0.3})$	$Mn^{+2}_{0.3}Fe^{+3}_{1.7}$
Mz1	$(Mn^{+2}_{0.8}Fe^{+3}_{0.2})$	$Mn^{+2}_{0.1}Zn^{+2}_{0.1}Fe^{+3}_{1.8}$
Mz3	$(Mn^{+2}_{0.6}Zn^{+2}_{0.1}Fe^{+3}_{0.3})$	$Mn^{+2}_{0.1}Zn^{+2}_{0.2}Fe^{+3}_{1.7}$
Mz5	$(Mn^{+2}_{0.5}Zn^{+2}_{0.2}Fe^{+3}_{0.3})$	$Zn^{+2}_{0.3}Fe^{+3}_{1.7}$
Mz6	$(Mn^{+2}_{0.4}Zn^{+2}_{0.4}Fe^{+3}_{0.2})$	$Zn^{+2}_{0.2}Fe^{+3}_{1.8}$
Mz7	$(Mn^{+2}_{0.1}Zn^{+2}_{0.7}Fe^{+3}_{0.2})$	$Mn^{+2}_{0.2}Fe^{+3}_{1.8}$
Mz9	$(Zn^{+2}_{0.9}Fe^{+3}_{0.1})$	$Mn^{+2}_{0.1}Fe^{+3}_{1.9}$

2.3 *Magnetization measurement*

The room temperature magnetic properties of the nanomagnetic particles were carried out up to 7500 Oe magnetic field using vibrating sample magnetometer (EG&G Model PAR 155) at 300 K. TGA technique is used to determine the temperature induced phase transition based on weight loss. Here we have modified this technique by applying external magnetic field to balance pan of TGA (Perkin-Elmer thermogravimetric analyser TGS-2) called MTGA. Uniform magnetic field was applied by keeping the balance pan in the centre of the two permanent magnets. Permanent magnet having 0·0150 T field strength was used. Prior to applying magnetic field, physical weight of sample was set to zero and finally magnetic field was applied and the change in the weight was recorded. Permanent magnet having a field strength of 0·0150 T was

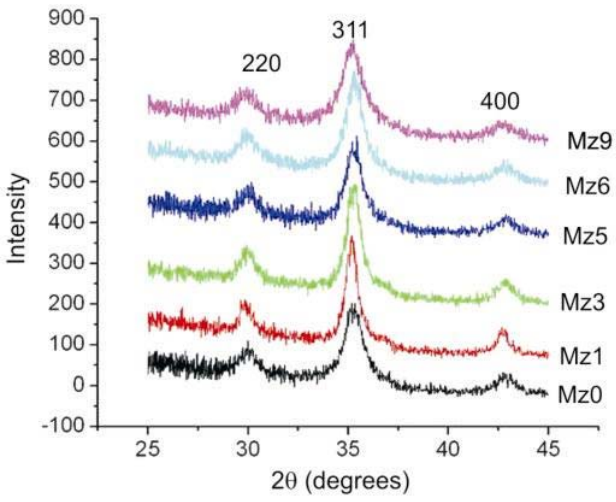

Figure 1. X-ray diffraction pattern of the nanosized $Mn_{1-x}Zn_xFe_2O_4$ ferrites.

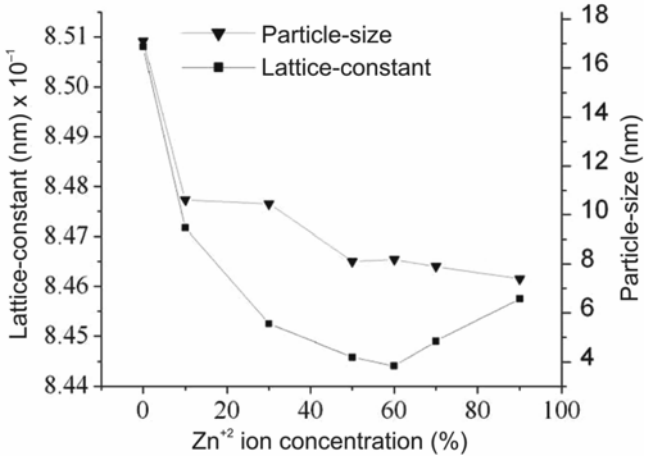

Figure 2. Variation of lattice constant and particle size with Zn doping.

Table 2. Cation distribution of $Mn_{1-x}Zn_xFe_2O_4$.

Sample	Zn doping (%)	ν_1 (m^{-1}) × 10^2	ν_2 (m^{-1}) × 10^2	*a*(nm)	*d*(nm)
Mz0	0	568	460	0·8508	17·1
Mz1	10	582	441	0·84717	10·61
Mz3	30	579	462	0·84525	10·45
Mz5	50	570	451	0·84458	8·108
Mz6	60	574	435	0·84441	8·18
Mz7	70	576	460	0·84900	7·90
Mz9	90	565	418	0·84575	7·39

used. Prior to applying magnetic field, physical weight of the sample was set to zero and finally magnetic field was applied to record magnetic weight. The data was recorded from 50–750°C. Temperature was increased in steps of 20°C.

The Curie temperature (T_C) was measured by plotting the magnetization vs temperature graph using MTGA. The a.c. magnetic susceptibility measurements were carried out using indigenously designed a.c.-susceptometer at 211 Hz frequency in temperature range of 80–300 K (Kalpesh *et al* 2004).

3.1 *X-ray diffraction analysis*

The sharp lines and absence of impurity peaks in the X-ray diffraction pattern (figure 1) indicates the formation of crystalline single-phase spinel structure. Figure 2 shows the lattice constant variation with Zn concentration. It is evident from the graph series decreases when the *x* value varies from 0 till 0·6 and it increases marginally from $x = 0{\cdot}7$ to $x = 0{\cdot}9$. The explanation for the above observed results can be given on the basis of the cation distribution among the A- and B-sites as given in table 1, which has been deduced from the preliminary information from the XRD intensity and IR spectrum.

The relative concentration of Mn and Zn in the ferrite structure not only influences the particle size and lattice parameter but also causes deviation in the distribution of cations at the lattice sites of the nanoparticles from that of the bulk. The resulting cation distribution is shown here to be a consequence of two competing processes: (a) the strong chemical affinity of certain cations to occupy either A- or B-sites and (b) the metastable cation distribution in nanoparticles. The situation becomes more complex when the stoichiometry is changed (Chandana Rath *et al* 2002). This may arise when large number of small ions replaces ions having large radii. Hastings and Corliss (1956) have shown from the neutron diffraction investigation of the polycrystalline manganese ferrite, that 81% of the manganese to be in the A-sites. Fe^{3+} ions prefer the A-sites but less compared to the Mn^{2+} ions.

The contribution of the B-site cations is $\sqrt{3}$ times more than that of the A-site cations in influencing the lattice constant. At the same time, as tetrahedral site is smaller than that of octahedral site, A-site will be affected more with the introduction of larger cations. The ionic radii of Mn^{+2}, Zn^{+2} and Fe^{3+} are 0·066 nm, 0·060 nm and 0·049 nm, respectively in the tetrahedral site and 0·083 nm, 0·074 nm and 0·055 nm, respectively in the octahedral site (CRC Hand Book).

There is also a systematic decrease in the particle size (d) as can be seen from table 2. The reduction in the physical dimension of a crystal lattice leading to a change in the lattice constants was recognized as far back as 1930, when Lennard–Jones made the conjecture that the unit cell should contract with decreasing size in ionic systems and expand in covalent ones.

The variation in the lattice constant can be explained by referring the cation distribution given in table 1. As the concentration of the Zn^{2+} ion increases from $x = 0$ to $x = 0{\cdot}1$, Mn^{2+} ion (0·066 nm) replaces the smaller Fe^{3+} ion (0·049 nm) in the A-site. The doped Zn^{2+} ion (0·074 nm) occupies B-site and the percentage of the Fe^{3+} ion (0·055 nm) increases marginally. This change causes contraction of the B-site and expansion of the A-site. The net effect of this change is a reduction in the lattice constant. On similar lines one can explain the systematic decrease in the lattice constant till $x = 0{\cdot}6$. For $x = 0{\cdot}7$, there is an unusual increase in the lattice constant. This is due to 100% occupancy of Zn^{2+} ion on the A-site. There is a negligible contraction of the A-site, while the B-site expands. This results in a slight expansion of the lattice constant. It is also observed that for $x = 0{\cdot}9$, there is a slight increase in the value of the lattice constant which can be similarly explained from the cation distribution given in table 1.

To account for the nanosized nature of the particles, it has been reported that the particle size of ferrites is influenced by the oxidation rate of the Fe^{2+} ions. In a reaction process where Fe^{3+} is involved, the precipitation rate has been found to increase, which results in very fine particles (Sheppard *et al* 1989; Chandana Rath *et al* 2002). In the co-precipitation synthesis route adopted for the present study, $FeCl_3$ was one of the constituents, the other two being $MnCl_2$ and $ZnSO_4$. Therefore, the presence of Fe^{3+} results in fine ferrite particles. However, this does not explain why the particle size depends on the composition when the preparation technique, synthesis tempera-

ture, and pH of precipitation are identical for all compositions (Schele and Deetscreek 1961).

This can be explained due to the strong chemical affinity of specific cations like Zn^{2+} to the tetrahedral A-site and the metastable cation distribution in nanoscale range of ferrite particles. Based on these features, one can explain the dependence of particle size on cation stoichiometry: The nucleation and particle growth during hydrothermal synthesis is a process that invokes absorption/desorption of ions and the occupancy of their specific sites. In a complex system like the ferrites where many cations are involved, the nucleation and growth of particles are expected to be influenced by the probability of a cation occupying available chemically inequivalent sites and by its affinity to these sites. In the case of $MnFe_2O_4$, Mn^{2+} does not have that strong preference of occupying only the tetrahedral site and a small fraction (< 20%) can occupy the octahedral site. Mn^{2+} will, therefore, have a higher probability of getting absorbed by a nucleus.

In spinel ferrites containing divalent cations, other than Fe^{+2} are formed by the dissolution–crystallization process (Jolivet *et al* 2006). In the case of MFe_2O_4, M^{2+} and Fe^{3+} ions simultaneously undergo the hydrolysis process leading to the formation of sparingly soluble hydroxides, which later condense to thermodynamically stable oxides. Therefore, it is expected that the K_{SP} (solubility product constant) values of both elements can influence the precipitation process. Since the ferrihydrate process is common in all ferrite ions, the size variation can be attributed to K_{SP} values of $M(OH)_2$. The K_{SP} value of Mn^{2+} are higher than that of Fe^{3+}, while K_{SP} value of Fe^{3+} is higher than that of Zn^{2+} (Gyanprakash *et al* 2007).

Since the K_{SP} of Zn^{2+} is lower than Fe^{3+}, the growth of $ZnFe_2O_4$ nuclei will be restricted. Based on the above arguments, we can understand the decrease in the particle size with the increase in the Zn^{2+} doping.

3.2 *Infrared spectrum analysis*

Far infrared absorption spectroscopy is an excellent tool to study the distribution of the cations in the tetrahedral and octahedral sites in ferrite system. The IR absorption band changes with the change introduced in the A-site and B-site cation distributions in the ferrite system. It is also used to determine the local symmetry in crystalline solids, ordering phenomenon in spinels and presence/absence of Fe^{+2} ions. It can also be used to determine the force constants and elastic moduli (Waldron 1955; Ravinder and Manga 1999; Ladgaonkar *et al* 2002) of ferrite systems.

The IR absorption band for the $Mn_{1-x}Zn_xFe_2O_4$ series is shown in figure 3. The room temperature (300°K) IR spectra for the Mn–Zn ferrites are shown in figure 1 above. Two absorption bands below 1,00,000 m^{-1} is a common feature of all the ferrites. The bands arise from the lattice vibrations of the oxide ions against the cations. The bands in the 30,000–70,000 m^{-1} region are assigned to the fundamental vibrations of the crystal lattice (Waldron 1955; Amer *et al* 2003; Hameda *et al* 2004). The band around 60,000 m^{-1} is attributed to stretching assigned to a vibration of the coordinated group(s) containing the highest valency cation (Tarte and Preudhomme 1971). The presence of the divalent ions explains the presence of the weak bands (Wei *et al* 2001). The cation distribution given in table 1 is deduced on the basis of the IR spectral absorption band of the samples after getting preliminary information from the XRD intensity calculations.

3.2a *Explanation of ν_1 band*: This band exists between 57,000 m^{-1} and 58,300 m^{-1}. It has been observed that the ν_1 band continues to shift towards the higher values up to $x = 0{\cdot}2$. This can be explained from the fact that the Fe^{3+}–O^{2-}

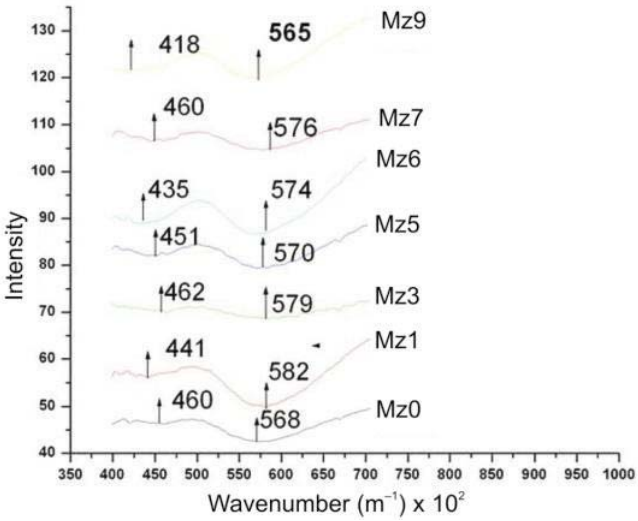

Figure 3. IR pattern of the $Mn_{1-x}Zn_xFe_2O_4$ ferrites.

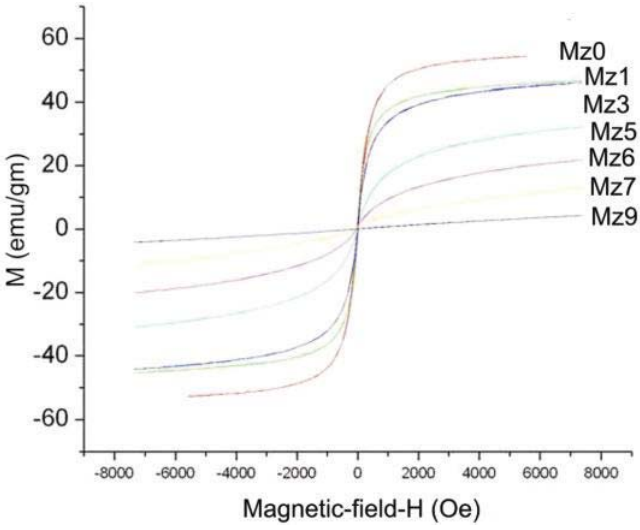

Figure 4. VSM magnetization data of $Mn_{1-x}Zn_xFe_2O_4$ ferrites at 300°K.

bond is shortened due to replacement of the smaller Fe^{3+} ion or ions (ionic radii = 0·049 nm) by the bigger Zn^{2+} (ionic radii = 0·060 nm) ion or Mn^{2+} ion (ionic radii = 0·066 nm) in the A-site. The resonant frequency has inverse relationship with the bond length. The ν_1 band decreases at $x = 0{\cdot}3$, since Fe^{3+} ion replaces a bigger Mn^{2+} ion at the A-site (ionic radii = 0·066 nm) and Zn^{2+} ion replaces a Mn^{2+} ion. The ν_1 band decreases marginally for $x = 0{\cdot}5$, since Zn^{2+} ion replaces Mn^{2+} ion at the A-site, which have nearly same ionic radii. For $x = 0{\cdot}6$, Zn^{2+} ion replaces a smaller Fe^{+3} ion, thereby resulting in the migration of Fe^{3+} ion from the A-site towards the B-site and another Zn^{2+} ion replaces Mn^{2+} ion. The net effect of this substitution results in a marginal increase in the ν_1 band. A very little change is observed for $x = 0{\cdot}7$ since Zn^{2+} ions replace Mn^{2+} ions. At $x = 0{\cdot}9$, there is a decrease in the value of ν_1, which can be explained on similar lines from the cation distribution given in table 1.

3.2b *Explanation of ν_2 band*: The ν_2 band is due to the vibration of the metal–oxygen bond in the octahedral site of the ferrite system. This band lies in the 41,800–46,400 m^{-1} range for the $Mn_{1-x}Zn_xFe_2O_4$ mixed ferrite samples. The band values are less compared to that of the ν_1 band. This is due to the fact that the tetrahedral site dimension is less compared to the octahedral site dimension and the absorption band has an inverse relationship with the bond length.

The explanation of the ν_2 band can be given on similar basis as given for the ν_1 band, based on the cation distribution given in table 1. The ν_2 band is due to Fe^{3+}–O^{2-} bond as explained earlier. The increase or decrease in the ν_2 band is due to the fact that there is a decrease or increase in the Fe^{+3}–O^{-2} bond length as a result of doping of Zn^{2+} ions. The ν_2 band decreases for $x = 0{\cdot}1$, since a smaller Fe^{3+} ion (ionic radii = 0·055 nm) replaces a bigger Mn^{+2} ion (ionic radii = 0·083 nm) as well as a smaller Zn^{2+} ion (ionic radii = 0·074 nm) replaces a bigger Mn^{+2} ion. The variation in the ν_2 band for other ferrite samples can be similarly explained from the cation distribution given in table 1. It can be seen from the graph that there is no regular pattern as far as the variation in the ν_2 band is concerned. This clearly proves that the Zn^{2+} ions does not occupy the A-site alone, but also has its presence in the B-site, which is also explained from the XRD analysis.

Table 3. Magnetization value (M_s) and Curie temperature (T_C) of $Mn_{1-x}Zn_xFe_2O_4$ samples.

Sample	Zn doping (%)	M_s (emu/g)	(T_B)K	(T_C)°C
Mz0	0	58·72	–	446
Mz1	10	51·01	–	314
Mz3	30	48·78	240	216
Mz5	50	38·95	140	173
Mz6	60	28·75	110	–
Mz7	70	19·55		–
Mz9	90	7·44		–

3.3 *Analysis of magnetization result*

Table 3 shows the comparison of the magnetization values (M_s) for the $Mn_{1-x}Zn_xFe_2O_4$ series. The field dependence of the magnetization of the $Mn_{1-x}Zn_xFe_2O_4$ series was measured using a vibrating sample magnetometer (VSM) at 300°K with an applied field $-7{\cdot}5$ kOe $\leq H \leq 7{\cdot}5$ kOe. A variation of magnetization with the applied field at a temperature of 300 K is presented in figure 4, where the typical characteristics of superparamagnetic behaviour like the absence of hysteresis, almost immeasurable coercivity, remanence and the non-attainment of saturation even at a high magnetic field of 7·5 kOe are observed.

The non-saturation of M–H loop and the absence of hysteresis, remanance and coercivity at 300 K are indicative of the presence of superparamagnetic and single domain particles for the ferrite materials (Liu and Fu 2007). The explanation for the decrease in the M_s value with the increase in the Zn^{2+} ion doping in the $MnFe_2O_4$ ferrite can be explained due to the following reason given below:

The decrease in the magnetization with the decrease in the particle size is due to the influence of the cationic stoichiometry and their occupancy in the specific sites (Chen *et al* 1996; Mahmoud *et al* 2000; Arulmurugan *et al* 2005). The variation of the saturation magnetization at room temperature with the Zn concentration is shown in table 3. The core-surface model can also explain the decrease in M_s samples with nanoparticles. In this model, the crystal grain can be divided into two parts, viz. the core and the surface layer, with significantly different magnetic properties. The magnetization for the surface layer is significantly smaller compared to the core. The decrease in the saturation magnetization of the surface layer has several potential sources, including crystal imperfection on the surface layer, reduction in super exchange interactions and noncollinear magnetic structure. The spins at the surface of the particles do not align completely in the direction of the applied magnetic field. The spin glass layer or magnetically dead layer having a thickness of about 0·6 nm was thought to be one of the reasons for the reduction of the saturation magnetization (Chen *et al* 1996; Martinez *et al* 1998). The core has a normal spinel crystal structure, in which the magnetic cations are ferrimagnetically ordered to form a single domain.

The major feature of the atomic configuration in the shell (surface) region lies in its less lattice periodicity. The magnetic cations in the shell possess less and variable coordination, which frustrates the super exchange interaction, resulting in a canted spin configuration in this region. In order to completely align all the spins in the shell region, a very high field has to be applied (of the order of 10^6 Oe). This is the reason a typical nanosized ferrite particle does not reach saturation under an applied

field. Therefore, the observed magnetization process of this system originates mainly from the domain rotation of the inner core region, while the spins in the shell have no major contribution to magnetization.

The zinc occupancy of the octahedral site is not unprecedented; this is considered as an indication of substantial cation disorder. As a result of the Zn ion being diamagnetic, it cannot participate in super exchange coupling between the octahedral and tetrahedral lattices; therefore, an inhomogeneous excess of zinc in the ferrite would disrupt some magnetic coupling and lead to an overall reduction in magnetism.

The variation of the Curie temperature with increasing Zn concentration is shown in table 3. We can see that there is a systematic decrease in the value of the Curie temperature (T_C) as the zinc concentration increases. This is due to the substitution of more non-magnetic Zn^{2+} ions instead of the magnetic Mn^{2+} ions. The value of T_C is found to be higher than that of its bulk counterpart. This is due to the deviation of cation distribution in a nano sized particle in comparison with its bulk counterparts (Chandana Rath *et al* 2002). In general, magnetic properties are controlled by exchange interaction of the metallic ions on the two interactive sublattices A and B. The change in T_C may be positive or negative depending on the boundaries, geometry, and interaction. It is also possible that T_C decreases due to some unknown surface effect. For small particles a significant fraction of atoms is on the surface, and it is reasonable to expect their magnetic interactions to be different. Hence a different average Curie temperature (Chen *et al* 1996). The graph of the variation of the magnetization with temperature for different samples is shown in figure 5 below. Many early workers (Wolski *et al* 1995; Chandana Rath *et al* 2002; Arulmurugan *et al* 2005) observed cusp (i.e. the magnetization increased beyond a point instead of approaching zero) in many samples in which the Zn concentration is more. They observed that the cusp was less pronounced for lower concentrations of Zn (Chandana Rath *et al* 2002; Arulmurugan *et al* 2005). We did not find any such cusp for the four different samples as can be seen from figure 5.

4. A.C. susceptibility measurements

The thermal variation of the real part of a.c. susceptibilities (χ^1) of the $Mn_{1-x}Zn_xFe_2O_4$ series is shown in figure 6. Here the Y-axis represents normalized readings with respect to the gram weight of the sample. The reduction in amplitude with the increase in the Zn concentration is due to the reduced value of magnetization. All the observed variations clearly indicate the presence of SPM phases in all the samples. It can be conjured that we might also get a similar SPM phase for Mz1 and Mz0 samples, if we go beyond 300 K.

The real part of a.c. magnetic susceptibility increases with the decrease of temperature and shows a maximum at temperature at the blocking temperature, T_B. Here the blocking temperature (T_B) is defined as the temperature at which the magnetic relaxation time of the particles equals to the experimental time scale of a.c. magnetic susceptibility, τ_0, of (1) given below.

$$\tau = \tau_0 \exp\left(\frac{K_A V}{kT}\right) \to 1.$$

In the ferrite samples under present study the χ^1 vs T curves give broad maxima indicating the presence of distribution of particle sizes in the samples. Here τ is the time scale of the a.c. magnetic susceptibility measurements, which was 4·7 ms and τ_0 has been taken as 10^{-9} s (Neel 1949; Chantrell and Wohlfarth 1983; Popplewell

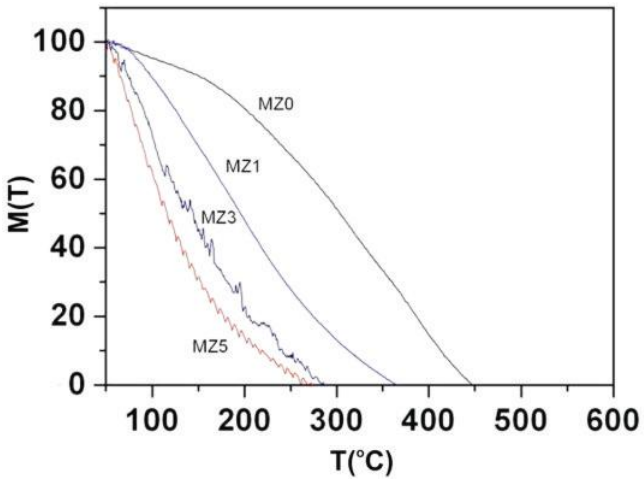

Figure 5. Magnetization variation of the $Mn_{1-x}Zn_xFe_2O_4$ ferrites with temperature.

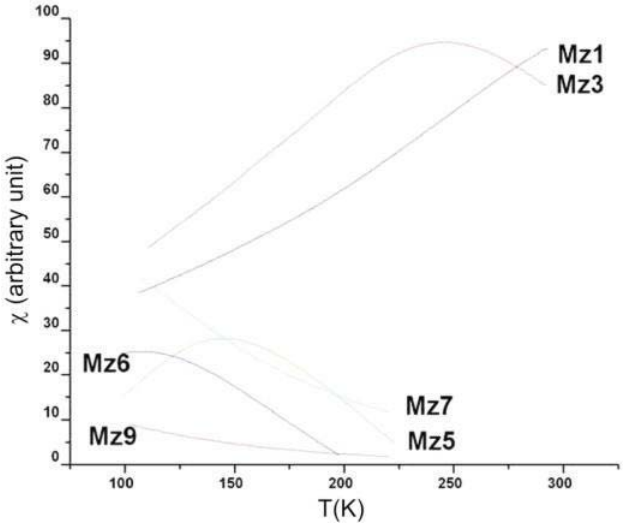

Figure 6. A.C. susceptibility response of $Mn_{1-x}Zn_xFe_2O_4$ ferrites with temperature.

and Sakhini 1995). Here the anisotropy constant, K_A, is the sum of magneto crystalline anisotropy due to dipole–dipole and/or interparticle exchange time scale interactions together with the shape and surface anisotropy of the nanoparticles. Above the blocking temperature the particles satisfying this relation will relax during the time scale of a.c. magnetic susceptibility measurements. Below the blocking temperature, the particles will be in a blocked state. It can be seen from table 3 that the blocking temperature (T_B) increases with the decrease in Zn ion concentration. This is due to the increase in the particle size. It needs more energy to flip a larger particle compared to a smaller particle. The stronger the dipolar interactions between the nanoparticles, higher are the blocking temperatures.

5. Conclusions

The IR spectrum and XRD of the Mn–Zn ferrite sample gives a clear indication of the formation of the ferrite phase for all samples. The lattice constant variation as well as the IR spectrum results quite agree with the cation distribution. It clearly points to the fact that the Zn^{2+} zigzags between the A and B sites for different proportions of zinc doping. The changes in the cation distribution due to the changes in the Zn^{2+} ion concentration are clearly reflected in the absorption band. The particle size reduces with the increase in the Zn^{2+} ion concentration, with the variation ranging from 12 nm to about 7 nm.

The mixed Mn–Zn ferrites can be tailored as per the requirements with respect to the value of the magnetization, Curie temperature, particle size as well as the blocking temperature. The characterization results can help in identifying the right combination of the Mn–Zn ferrite material.

Acknowledgement

One of the authors (RI) would like to thank Mr Vipul Davariya, Mr Mrudul Ghadvi and Ms Kinnari Parekh for extending help in the experimental process.

References

Amer M A 2003 *Phys. Status Solidi* **B237** 459
Arulmurugan R, Jeyadevan B, Vaidyanathan G and Sendhilnathan S 2005 *J. Magn. Magn. Mater.* **288** 470
Ataie A, Piramoon M R, Harris I R and Ponton C B 1995 *J. Mater. Sci.* **30** 5600
Chandana Rath, Anand S and Das R P 2002 *J. Appl. Phys.* **91** 2211
Chantrell R W and Wohlfarth E P 1983 *J. Magn. Magn. Mater.* **40** 1
Chen J P, Sorenson C M, Klabunde K J, Hadjipanayis G G, Delvin E and Kostidas A 1996 *Phys. Rev.* **B54** 9288
Grossinger R and Sanchez Li J L 2005 *J. Magn. Magn. Mater.* **294** 252
Gyanprakash. G, John Philip and Baldev Raj 2007 *Mater. Letts* **61** 4545
Hameda O M 2004 *J. Magn. Magn. Mater.* **281** 36
Hastings J M and Corliss L M 1956 *Phys. Rev.* **102** 1460
Herzer G, Vaznez M, Knobel M, Zhokov A, Reininger T and Davies H A 2005 *J. Magn. & Magn. Mater.* **294** 252
Jayadevan B, Tohji K and Nakatsuka K 1983 *J. Appl. Phys.* **22** 882
Jayadevan B, Tohji K, Nakatsuka K and Narayanasamy A 2000 *J. Magn. Magn. Mater.* **217** 99
Jolivet Jean-Pierre, Trone Elisabeth and Chaneac Corinne 2006 *C.R. Geoscience* **338** 488
Kalpesh H Jani, Upadhyay R V and Mehta R V 2004 *Indian J. Engg. & Mater. Sci.* **11** 349
Ladgaonkar B P, Kolekar C B and Vaingankar A S 2002 *Bull. Mater. Sci.* **25** 351
Liu X M and Fu Shao-Yun 2007 *Jmmm* **308** 61
Mahmoud M H, Hamdeh H H, Ho J C, O'Shea M J and Walker J C 2000 *J. Magn. & Magn. Mater.* **220** 139
Martinez B, Obradors X, Balcells Li, Rounet A and Monty C 1998 *Phys. Rev. Lett.* **80** 181
Moinuddin M K and Ramana Murthy S J 1993 *Alloys & Compounds* **194** 105
Mostafa A A, El-Shobaky G A and Girgis E 2006 *J. Phys. D: Appl. Phys.* **39** 2007
Neel L 1949 *Ann. Geophys.* **5** 99
Pankov V V, Pernet M, Germ P and Molard P 1993 *J. Magn. Magn. Mater.* **120** 69
Popplewell J and Sakhini L 1995 *J. Magn. Magn. Mater.* **149** 72
Ravinder D 1999 *Mater. Lett.* **40** 205
Ravinder D and Manga T 1999 *Mater. Lett.* **41** 254
Schele W J and Deetscreek V D 1961 *J. Appl. Phys.* **32** 235
Sheppard L M 1989 *Am. Ceram. Soc. Bull.* **68** 979
Tarte P and Preudhomme J 1971 *Spectrochim. Acta* **A27** 961
Thakur A and Singh M 2003 *Ceram. Int.* **29** 505
Thummer K P, Chhantbar M C, Modi K B, Baldha G J and Joshi H H 2004 *J. Magn. Magn. Mater.* **280** 23
Upadhyay R V and Mehta R V 1993 *Pramana – J. Phys.* **41** 429
Waldron R D 1955 *Phys. Rev.* **99** 1727
Wei Qiang-Min, Li Jain-Biao and Chen Yong-Jun 2001 *J. Mater. Sci.* 5115
Wolski W, Wolska A, Kaczmarek J and Piszora P 1995 *Phys. Status Solidi* **A152** K19